Directed Functional Connectivity by Variational Cross-mapping of Psychophysiological Variables

Ameer Ghouse[a], Johannes Schultz[b,c], Gaetano Valenza[a]

[a]*Research Center "E.Piaggio" School of Engineering, University of Pisa, Pisa, 56126, Italy*
[b]*Center for Economics and Neuroscience, University of Bonn, D-53113 Bonn, Germany*
[c]*Institute of Experimental Epileptology and Cognition Research, University of Bonn Medical Center, D-53113 Bonn, Germany*

Abstract

Classic methods of exploratory time-lag methods of directed connectivity hinge on wide-sense stationarity, which restricts their application to resting-state or time-windowed connectivity. Thus, nonlinear temporal effects in task-evoked neural activity observed in fMRI-BOLD data may be underestimated. Instead of a combinatorial search through dynamic causal models to account for such effects, we propose a modification of variational cross-mapping methods. We take inspiration from psychophysiological interactions to determine a priori covariance functions of nonparametric generative Gaussian process models to compare evidence of directional influence between paired regions of interest. To validate the method, we determine Bayes factors for correct inferred directionality in simulated bidirectional Lorenz-Rossler systems or neurovascular signals evoked by neural networks. We demonstrate that the method maintains strong evidence of correct event-coupling direction with high sensitivity and minimal specificity sacrifice. We further validate the method on a well-known object response dataset, by assessing whether it uncovers previously documented effective connectivity findings on face processing from BOLD responses mapped onto cortical surface parcellations of ventrolateral cortical areas. Our results agree with current effective connectivity findings about face processing, suggesting vertices of the inferior occipital gyrus send information to the superior temporal sulcus and the fusiform cortex, without direct connectivity between the fusiform cortex and the superior temporal sulcus.

1. Introduction

How does one determine coupling effects in a system invoked by a particular stimulus that is embedded in a sea of simultaneous interactions affecting an observed signal? How does one control for how past events affect a system's response to a stimulus? These are particular demands that functional coupling analyses of psychophsyiological variables in neuroimaging oblige. Such functional coupling in neuroimaging data is not only nonlinear but also has a complex nature due to its high dimensionality, which emerges from the many interactions and feedback loops in neural circuits [28, 25, 40, 53]. Coupling analysis in neuroimaging, hereon referred to as connectivity, can be divided into two camps; functional, and effective connectivity. Functional connectivity hinges on discovering statistical relationships between regions of interest, such as correlation [21, 20]. This kind of connectivity analysis, however, is prone to confounds as correlation can be either a chance occurrence, or may actual be conditionally independent. Furthermore, measures of correlation yield undirected measures of connectivity.

There have been extensions to assess functional connectivity in a directed manner. Psychophysiological interactions is one of these methods. It exploits general linear modeling and so-called psychophysiological interaction variables, which are constructed from the BOLD data and the timing of psychological events. It aims to uncover brain regions whose functional connectivity with a seed region changes depending on the occurrence of a psychological variable of interest [17, 47, 31]. However, this method takes no consideration of the direction of connectivity. Granger causality (GC), and its nonparametric counterpart transfer entropy, can take temporal precedent information into consideration. However, the method is inherently memoryless, and can thus not handle nonlinear and temporal context-dependent effects observed in neural data [60, 57, 10, 15, 16].

On the other hand, effective connectivity attempts to ascertain the mechanistic properties of a network, or in other words the influence of one neural system on another [20]. Dynamic causal modeling is a particular effective connectivity method that can take into consideration the nonlinear interactions in time of a system, and how coupling may emerge from it. However, such a method requires an exhaustive combinatorial search of candidate models in order to select the one with the most evidence given a priori expectations [16]. There have been developments to the DCM framework to make it more appropriate for whole-brain exploratory analysis, particularly regression DCM [14], though this method comes at the sacrifice of high order nonlinear characterizations of coupling in order to allow computational feasibility. Methods that are more adept

Email address: a.ghouse@studenti.unipi.it (Ameer Ghouse)

for exploratory analysis, such as Granger causality or transfer entropy, do not have inherent structures to impose a priori knowledge of when task events occur, and are reliant on assessing time series on windows. Such methods thereby ignore crucial effects that emerge from dynamic complex effects such as memory, as determined by location in state space. Granger causality and transfer entropy also have the potential to dictate false positive directions of influence [51, 50].

Recently proposed probabilistic models of cross-mapping effects [54], i.e. Gaussian process convergent cross mapping (GP-CCM) [29, 30], utilizes a posteriori strength of evidence with subsequent significance of statistics given by the approximated a posteriori distribution of hyperparameters and permutations of state space reconstructions. Inherently, probabilistic models offer a high degree of flexibility to dictate the structure of the model under investigation by specification of a priori effects. Thus, to alleviate issues of state of the art methods mentioned above, we propose determining cross-mapping between multivariate psychophysiological interactions between regions of interests with a specified a priori covariance function that allows focusing on cross-mapping effects during events of interest while taking in consideration covariance of states outside the task window. Effectively, we develop a nonparametric probabilistic generative model comparison for task-dependent activity in the brain. We validate the method both on simulations of bidirectionally coupled Lorenz-Rossler systems, neural networks transformed by nonlinear hemodynamic responses, as well as on a publicly available face perception dataset [34]. Regarding the face perception dataset, the proposed method should replicate findings of network interactions previously reported in dynamic causal modeling studies [12]. Specifically, we expect to identify a connection from face-sensitive parts of the inferior occipital gyrus to the superior temporal sulcus and fusiform gyrus.

2. Methods

3. Data and Code Availability Statement

All code used for simulating, obtaining, or processing data can be found in the following GitHub repository: https://github.com/lemiceterieux/PPI-GP-CrossMapping.

3.1. Constructing Embeddings from Psychophysiological Interactions

Here, we introduce how variational Gaussian Process Convergent Cross-Mapping (VGP-CCM) can be applied to discover how task dependent coupling between regions of interest by exploiting psychophysiological interaction methods [17]. We denote the Psychophysiological Interactions (PP) as $H(p_i \times H^{-1}x_{mk}) = PP_{mik}$ where p_i designates the ith Psychological Interactions (P) event based on the experimental paradigm, H the hemodynamic response function in a Toplitz matrix form [31], and x_{mk} the kth volumetric voxel (or surface vertex) of the mth region–the physiological event. Note, for neuroscientific imaging modalities that operate directly at the neural time scale, like EEG, the hemodynamic response function is not needed (or seen as an identity matrix). Regarding the psychological variable P, If consideration is made for comparing differences between an event 1 and event 2, the P would be constructed similar to [23], where event 1 would be valued 1 at its timing, -1 at event timings of event 2, and zero elsewhere. If, otherwise, the interest is the effect of the cross-mapping just for event 1, the P would be 1 at the psychological event 1 timing, and -1 everywhere else [24]. In this paper, we invoke the second method in order to glean psychophysiological interactions between regions of interests during a singular event, obtaining a connectivity matrix S_1, for example during an event 1. To get marginal representations of connectivity during event 1 given knowledge of event 2 connectivity, we obtain $S_{1|2...E} = S_1 \underset{i=2...E}{\wedge} \sim S_i$ where E signifies E events. Each region (whether it's a searchlight or a region selected from an atlas) would correspond to M multivariate time series. Thus, we need to consider multivariate generalization of reconstructions of the state space, as specified in [9]. Explicitly, the delay-coordinate embedding, given an embedding dimension of μ and lag time τ, is:

$$\begin{aligned}\mathcal{M}_{PP_{mit}} = \{&PP_{mi0t}, PP_{mi0t-\tau}, ..., \\ &PP_{mi0t-\mu\tau}, PP_{mi1t}, PP_{mi1t-\tau}, ..., \\ &PP_{mi1t-\mu\tau}, PP_{mi2t}, ..., PP_{mikt-\mu\tau}\}\end{aligned} \tag{1}$$

3.2. Preserving Dynamics in Dimensionality Reduction

The dimensionality of the state space scales linearly with the amount of time series obtained, having an embedding dimension of $k\mu$. Distances in such high dimensions in turn end up being almost meaningless as the ratio of distances between closest and farthest neighbor approach almost 1 [1]. This would render a radial basis function kernel like the one we use very poor at uncovering covariance between samples. We instead find a projection that reduces the dimensionality of the multivariate time series. Furthermore, we wish to determine a projection that is differentiable in order to preserve flow dynamics [3]. That is:

$$\begin{aligned}Z_{mit} &= \psi(PP_{mit}) \\ \frac{dZ_{mit}}{dt} &= \frac{d\psi(PP_{mit})}{dt} \quad = \frac{\partial\psi(PP_{mit})}{\partial PP_{mit}}\frac{dPP_{mit}}{dt}\end{aligned} \tag{2}$$

This implies that ψ needs to preserve temporal structure, achievable if it is differentiable with regards to its input PP. PCA is one popular method transform that is differentiable as it's a linear function. Though there are also popular nonlinear dimensionality reduction techniques such as UMAP or Ivis that are very popular in machine learning, they do not provide a metric for how much variance is preserved in their embedding, thus no knowledge is provided for how much information is lost in the reduction [43, 55]. Thus we used PCA for our dimensionality reduction of the multivariate time series extracted from a parcel of interest. For the sake of conciseness, we refer to manifolds reconstructed by a psychophys-

iological interaction at region of interest m, PP_{mi} even after dimensionality reduction as $\mathcal{M}_{PP_{mi}}$. Thus, the formulation of VGP-CCM in its entropy interpretation is testing $H_o : H(\mathcal{M}_{PP_{1i}}|\mathcal{M}_{PP_{2i}}) = H(\mathcal{M}_{PP_{2i}}|\mathcal{M}_{PP_{1i}})$ with $H_1 : H(\mathcal{M}_{PP_{1i}}|\mathcal{M}_{PP_{2i}}) < H(\mathcal{M}_{PP_{2i}}|\mathcal{M}_{PP_{1i}})$ if an ROI X_1 couples in in the direction towards X_2 during event i. We use α to designate the first level significance level for rejecting the null hypothesis on a subject level.

3.3. Choosing the VGP-CCM A Priori Functions

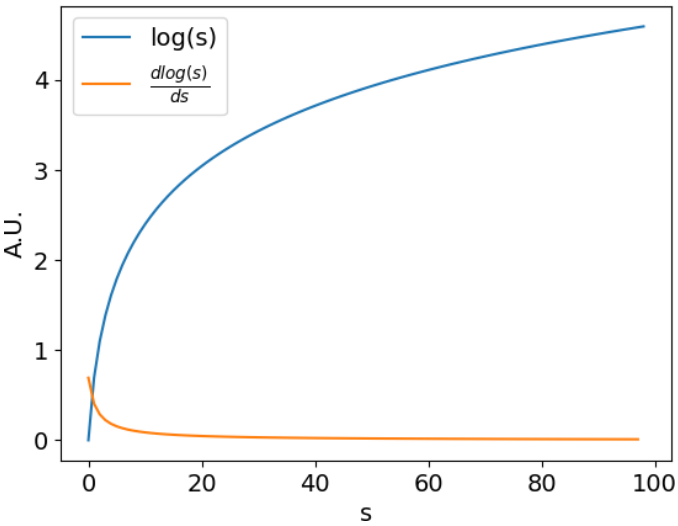

Figure 2: Plot of the logarithm of some argument s and its derivative. This illustrates the effect of modifying the diagonal elements of the a priori covariance kernel, which similarly affects its eigen-values that are most sensitive to components regarding the time point at those diagonal elements, during psychophysiological interaction cross-mapping. This in turn allows the ELBO for the approximation distribution $Q(\theta) \approx P(\theta|\mathcal{M}_{PP_{im}})$ to be optimized for the psychophysiological interaction condition of interest.

In order to have the VGP-CCM model focus on cross-mapping particularly for the psychological event of interest, we need to encode the event's unique nonstationary behavior. There are two ways to approach this; one is electing to choose a mean function of the psychophysiological event to be the physiological event itself. If a psychological event is centered, all timings off the psychological event of interest would have negative polarity and on the timing of the psychological event would have positive polarity. Thus, a probability distribution such as $P(\mathcal{M}_{PP_{mi}}|\theta_{mi}) = \mathcal{N}(\mu = \psi(x_{mi}), \Sigma = K(\mathcal{M}_{PP_{mi}}, \mathcal{M}_{PP_{mi}})|\theta_m i)$ encodes lower probability density of a PP during off events, and higher probability density during on events. In the language of dynamic causal modeling [18], off timings of psychological event timings would relate to latent connectivity and on psychological event timings would reflect induced connectivity by the psychological event. The second option that would provide a similar effect would instead be arrived at adding the squared difference between the physiological interaction and the PP to the a priori covariance function thus directly encoding the heteroskedastic nature of the psychophysiological event in the time series. This is similar to an a priori Gaussian process $P(\mathcal{M}_{PP_{mi}}|\theta_{mi})P(\mathcal{M}_{PP_{mi}}|PP_m)$ where $P(\mathcal{M}_{PP_{mi}}|PP_m) \sim \mathcal{N}(0, \sigma_p diag(d(\psi(x_{mi}), \psi(PP_{mi}))))$ where d is some distance or radial basis function. We can include σ_p in the hyperparameter variational function to optimize with the evidence lower bound in VGP-CCM. The radial basis function can also be parameterized by its own length parameter l_p similar to the usual automatic relevance detection kernel used in Gaussian processes [42]. The new covariance function is then:

$$\begin{aligned} K(PP_{mi}, PP'_{mi})^* = K(PP_{mi}, PP'_{mi}) \\ + \sigma_p diag(d(\psi(PP_{mi}), \psi(x_{mi}), l_p))) \end{aligned} \tag{3}$$

This modification for nonstationary effects on the diagonal of the covariance matrix encodes more information to characterize a cross-mapped state. By the nature of logarithms (as the entropy of multivariate Gaussians scales with the logarithm of the determinant of the covariance [2]), the local change of information when cross-mapping during time points off the psychological event encodes high entropy, and the derivative with respect to the argument in this regime is low, thus minimally affecting the result of cross-mapping compared to time points during the psychological event (see fig. 2). From our experiments, we found that cross-mapping the PP gave best results approaching it from modifying the a priori covariance function. This conditioning of the diagonal of the prior covariance matrix can also be seen as encoding information off the psychological event timings as confounds for inferring strength of coupling between regions of interest. As such, any other confounding variable can be modeled similarly, as $P(\mathcal{M}_{PP_{mi}}|C_k) \sim \mathcal{N}(0, d(\psi(x_{mi}), \psi(C_k)))$ where C_k is the kth confound. Then, the a posteriori approximation $Q(\theta_{mi}) \approx P(\theta_{mi}|\mathcal{M}_{PP_{mi}})$ will maximize the evidence for $P(Z_{mi})$. We test coupling between all regions m, i.e. $\kappa(\mathcal{M}_{PP_{1i}}, \mathcal{M}_{PP_{2i}})$ for a psychological event i as according to eq.

4.

$$\begin{aligned} \kappa(\mathcal{M}_{PP_{1i}}, \mathcal{M}_{PP_{2i}}) &= \frac{\int P(\mathcal{M}_{PP_{2i}}|\theta_{x1})P(\theta_{x1}|\mathcal{M}_{PP_{1i}})d\theta_{x1}}{\int P(\mathcal{M}_{PP_{1i}}|\theta_{x2})P(\theta_{x2}|\mathcal{M}_{PP_{2i}})d\theta_{x2}} \\ &= \frac{P(\mathcal{M}_{PP_{2i}}|\mathcal{M}_{PP_{1i}})}{P(\mathcal{M}_{PP_{1i}}|\mathcal{M}_{PP_{2i}})} \\ &\approx \frac{\int P(\mathcal{M}_{PP_{2i}}|\theta_{x1})Q(\theta_{x1})d\theta_{x1}}{\int P(\mathcal{M}_{PP_{1i}}|\theta_{x2})Q(\theta_{x2})d\theta_{x2}} \end{aligned} \tag{4}$$

3.4. Network-based Statistic Group Analysis

Correcting for multiple comparisons in exploratory connectivity analysis is an understudied field [38]. In dynamic causal modeling, empirical Bayes is used to compare competing models [59]. However, this does not apply here as exploratory methods are designed to be model-free. Other connectivity methods such as psychophysiological interactions in its GLM form or Granger causality restrict the search space to certain regions of interest rather than doing whole brain connectivity analysis as performed here , thus reducing the multiple comparisons factor in Bonferroni or False Detection Rate. There is, however, the family of Network Based Statistics (NBS) that assess a global statistic in order to correct for multiple comparisons [58]. Thus,

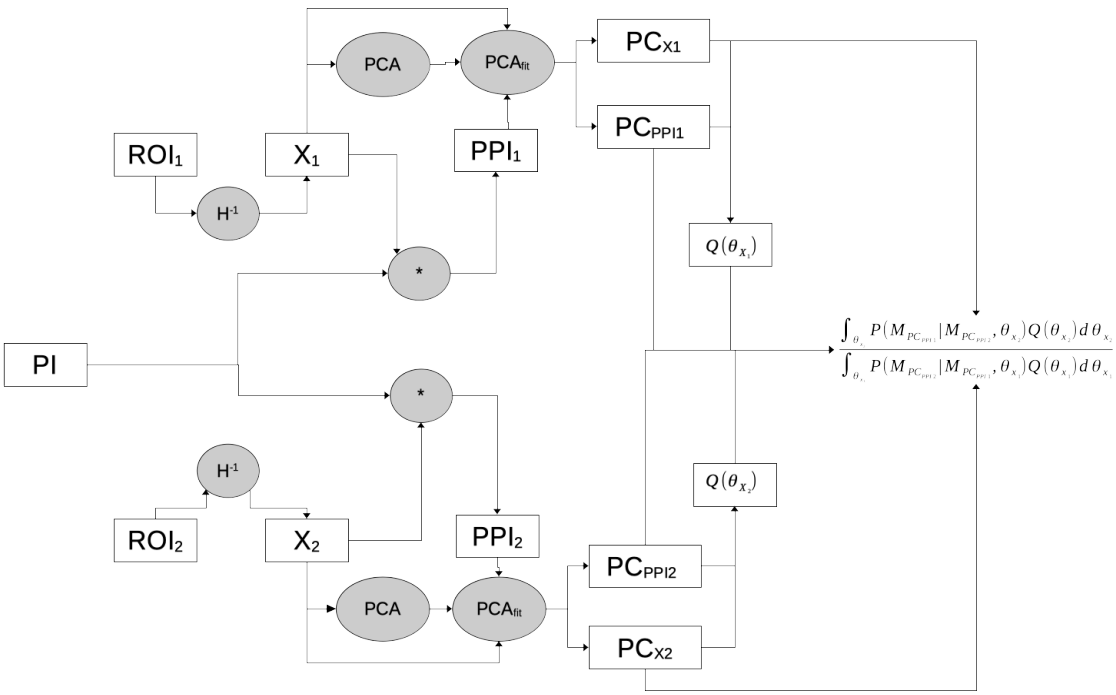

Figure 1: Block diagram of the PPI GP-CCM processing to arrive at the eventual coupling measure defined by the probability ratio.

instead of settling for using Bonferroni or other methods that do not take into consideration the structure of the data, we propose a global statistic of the connectivity network by exploiting the adjacency matrix and a notion of entropy on directed acyclic graphs as a modified form of NBS.

An adjacency matrix (S), i.e. a (0,1) matrix describing connections–where rows are edges coming out of a graphical node, and columns are edges coming into a node–is obtained from a hypothesis test (for the sake of explanation, consider a binomial test on a group analysis) to decide whether a positive connectivity was significant in the group. S_{ij} are connections in the adjacency matrix, with i denoting edges coming out of a node, i.e. outflow of information, and j denoted edges coming into a node, i.e. inflow of information. The matrix is 1 where an edge is significant and 0 when not significant decided by the group level significance test. The probability of an outgoing connection from node a given the network S is:

$$p(a|S) = \frac{\sum_{n=1}^{N} S_{an}}{\sum_{k=1}^{K}\sum_{n=1}^{N} S_{kn}} \tag{5}$$

While the probability of a connection coming into node b is:

$$p(b|S) = \frac{\sum_{n=1}^{N} S_{nb}}{\sum_{k=1}^{K}\sum_{n=1}^{N} S_{kn}} \tag{6}$$

Shannon entropies for edges coming out of a node, edges coming into a node, or the edge graph entirely would be:

$$\begin{aligned} H(out|S) &= \sum_{a=1}^{A} p(a|S) log(p(a|S)) \\ H(in|S) &= \sum_{b=1}^{A} p(b|S) log(p(b|S)) \\ H(joint|S) &= \sum_{a=1}^{A}\sum_{b=1}^{B} p(a,b|S) log(p(a,b|S)) \end{aligned} \tag{7}$$

Where $p(a,b|S) = p(a|S)p(b|S)$. Null distributions are bootstrapped for $H(joint|S)$.

We used a bootstrap analysis as according to [11, p. 226] to compute significance values for entropy. That is, we compute a "null" distribution of networks $\tilde{S}$ and see whether our entropy is significantly greater than the null. The bootstrap distribution is created by first obtaining a Binomial test p value matrix B with $\pi_o = 50\%$ for each connection (having binarized significant and non significant results from the VGP-CCM test). The true connectivity matrix S is created from the p value matrix B. We then create surrogate data by selecting 1000 new samples of the subjects VGP-CCM matrix via the plug-in principle described in [11]. Thus we obtain null data sets where the ith plug-in resample of the VGP-CCM matrix is $X'_i = X'_i - X_{\pi_o}$, where X_{π_o} is the VGP-CCM value which $1-\pi_o$ of the subjects are less than (thus, we have surrogate samples of connectivity where the $E(X' > 0) = \pi_o$). Then we calculate p values from a group level hypothesis test to obtain a surrogate p value matrix B' and obtain an adjacency matrix S' using a threshold on B' with $p < \alpha_n$. From there, we can create a null entropy distribution for $H(joint|\tilde{S})$ and obtain a p-values as:

Lorenz	σ_L	dt	σ	β	ρ	Rossler	σ_R	dt	ω_1	ω_2	a	b	c
	10^{-5}	0.1	10	$\frac{8}{3}$	28		10^{-5}	0.1	1.015	0.918	0.15	0.2	10

Table 1: Parameters of the Lorenz-Rossler systems

$$p_{joint} = \frac{\sum_{n=1}^{1000} I(H(joint|\tilde{S} = S) > H(joint|\tilde{S} = \tilde{S}_n))}{1000} \tag{8}$$

Where I(condition) is 1 when true, otherwise 0. p_{joint} provides a global test that confirms whether the entire graphical network itself is significant, thus $p_{joint} = p_{fwe}$. Thus, we can control for multiple comparisons in the t-test by choosing an α where $p_{joint} < 0.05$. We iteratively adjust $\alpha_n = \alpha_{n-1}/2$ with $\alpha_0 = 0.05$ until we reach the desired p_{joint}.

3.5. Simulated Unidirectional Lorenz-Rossler Systems With Randomly Induced Coupling

In order to validate the task-dependent variation of VGP-CCM. We simulated 50 realizations of a Lorenz-Rossler system with randomly switching coupling governed by the time event of a Psychological Interactions (P). Coupling strength parameters ϵ_x and ϵ_y control the degree to which a psychophysiological interaction couples to another "physiological" component. The parameter ϵ_y is fixed to 1, while coupling value is varied from $\epsilon_x = \{0, 1, 2, 3, 4\}$. Each realization is an integration of system equations from time t=0 seconds to t=100 seconds. 10 events for Y driving X (PI_{yx}) and X driving Y (PI_{xy}), i.e. induced connectivity from a psychological event, were simulated at random time points in each realization with duration 2 seconds. The system equations are as follows:

$$\begin{aligned}
dX_0 &= (\sigma(X_1 - X_0) + PI_{yx}(t)\epsilon_y X_0(Y_0 - 1))dt + \sigma_L(t)dW_{X1} \\
dX_1 &= (X_0(\rho - X_2) - X_1)dt + \sigma_L(t)dW_{X2} \\
dX_2 &= (X_0X_1 - \beta X_2)dt + \sigma_L(t)dW_{X3} \\
dY_0 &= (-\omega_2 Y_1 - Y_2 + PI_{xy}(t)\epsilon_x Y_0(X_0 - 1))dt + \sigma_R(t)dW_{Y1} \\
dY_1 &= (\omega_2 Y_0 + aY_1)dt + \sigma_R(t)dW_{Y2} \\
dY_2 &= (b + Y_2(Y1 - c))dt + \sigma_R(t)dW_{Y3}
\end{aligned} \tag{9}$$

The series X0 to X2 are part of the Lorenz system of equations; the series Y0 to Y2 comprise the Rossler equations. ϵ_x controls the nonlinear and synergistic coupling with the Rossler system at node Y_0 which propagates to the rest of the system of equations. Similarly, the Rossler equations can propagate through the Lorenz system of equations X through X_0 by ϵ_y in a similar fashion. W is a 6 dimensional Wiener process that we integrate our systems of equations with to simulate process dynamic noise. Finally, once we obtain series X and series Y, we add unit Gaussian noise $Z \sim \mathcal{N}(0, I)$ to simulate observation noise from a measurement such as fMRI, such that $X' = X + Z$ and $Y' = Y + Z$. The parameters of the systems can be seen in the table 1. Initial values at time $t = 0$ of the coupled system are randomly drawn as $X(t = 0) \sim \mathcal{N}(1, I)$ and $Y(t = 0) \sim \mathcal{N}(1, I)$.

From these simulations, the objective is to determine how well task-dependent VGP-CCM can disentangle the Lorenz equations forcing a Rossler system during the psychological events PI_{xy}, where Lorenz coupling strengths comprised $\epsilon_x = \{0, 1, 2, 3, 4\}$. Specificity, sensitivity and the Bayes factor were used as quality metrics. Specificity assesses how well the method avoids type I errors, and is calculated as $specificity = \frac{\text{True Negatives}}{\text{True Negatives + False Positives}}$. Specificity can also be seen as the probability $(-|M = -)$. Sensitivity, on the other hand is $p(+|M = +) = \frac{\text{True Positives}}{\text{True Positives + False Negative}}$. In summary, sensitivity can be seen as the probability that there truly was coupling in a specified direction given our model detecting so exists. On the other hand, specificity can be seen as the probability of the of there truly being no coupling given the model stating no coupling. From specificity, the probability $p(-|M = +)$, i.e. there actually being no coupling even when the model gives a positive result, can be calculated as $1 - p(-|M = -)$. Then, the Bayes factor for assessing posterior odds of positive coupling can be obtained as

$$BF(+) = \frac{p(+|M = +)}{p(-|M = +)} \tag{10}$$

In the simulations, We use the zero coupling positive rate to calculate $p(-|M = +)$. Given BF is a probability ratio, it can be read in odds form. For example, BF=21 would be interpreted as there being 21 positive coupling results to 1 negative coupling result if the model predicts positive, i.e. 20:1. Thus, BF can be seen as quantifying the factor by which we can improve our prior odds of there truly being coupling to obtain a posteriori odds. For example, if a priori odds of there being coupling was set to 1:9, i.e. 10% prior probability, the a posteriori odds of there truly being coupling, with Bayes factor=21, would be 21:9, i.e. 70% probability a posteriori, raising our confidence substantially.

3.6. Simulation of Neurovascular Signals Induced by Neural Networks

In order to assess the validity of the proposed PPI VGP-CCM on neural induced signals elicited such as those in functional near infrared spectroscopy (fNIRS) or functional magnetic resonance imaging (fMRI), we exploit forward models of hemodynamics to simulate neurovascular signals emerging from neural networks [52]. In these simulations we have network 1 and network 2 comprising a population of 50 neural units respectively. As per [52], a bilinear state equation is used to model metabolic demand signals (x) induced by a cognitive stimuli.

$$\dot{x} = Ax + \sum_{j=1}^{m} u_j B^j x + Cu \tag{11}$$

The A matrix describes the autonomous dynamics of the system; in our simulations, we treat it as a diagonal matrix with values -1, implying dynamics returning to a baseline 0 state. u are stimuli of a cognitive condition (where the element u_j is 0 when jth event is not occurring, and 1 when the jth event is occurring). B^j describes the interconnectivity between networks

of interest (i.e. $\begin{bmatrix} R_{11} & R_{12} \\ 0 & R_{22} \end{bmatrix}$ for network 1 causing network 2, and each R_{ij} is an i.i.d. random matrix $R_{ij} \sim \mathcal{MN}(0,1,1)$). The B matrices do not change in time, rather they are realized for each simulated time course. C describes which networks the stimulus condition interacts with, which in this paper, simulated as a diagonal matrix.

We perform 4 different simulations with three conditions u_1, u_2 and u_3. For simulation 1, u_1 and u_2 are events that occur 10 time each over a period of 1000 seconds; each event lasts 6 seconds on intervals of 1 minute. u_1 invokes network 1 to network 2 interactions via a random matrix, $R^1_{12} \sim \mathcal{MN}(0,1,1)$ while u_2 does not invoke interaction between the networks, i.e. $R^2_{12} = 0$. For simulation 2, $R^2_{12} \sim \mathcal{MN}(0,1,1)$ is instead inducing connections between network 2 to network 1. Event timings can be seen in 3a.

In simulation 3 and 4, u_1 and u_2 are events that occur within 20 times with stimulus duration of 6 seconds, and a short interevent time interval of 4 seconds (within the traditional peak time of the canonical linear hemodynamic response function [32]). Each pair of events are separated by 1 minute. The order of events are randomized for each pairing. Similar to simulations 1 and 2, simulations 3 and 4 either have u_2 not induce any network interactions, or has u_2 inducing connectivity between network 2 to network 1 respectively. Event timings can be seen in fig. 3b.

u_3 in all simulations is a binomial point process with $p = 0.3$ that describes random neural activity that elicit no functional interconnectivity between networks 1 and 2, i.e. $R^3_{12} = R^3_{21} = 0$. This serves as background noise on top of the activities.

After the neural state equations, regional blood flow f, blood volume v, and deoxyhemoglobin concentration q is simulated using the proposed parameters and mechanistic equations in [52]. A corrupted deoxyhemoglobin vector $q* = q+\epsilon$, where ϵ is additive noise sampled from $\mathcal{N}(0, 0.1I)$, is saved for further processing. Such processing comprises deconvolution (see fig. 3c and d), PCA dimensionality reduction of networks, and PPI VGP-CCM analysis.

Similar to the Lorenz-Rossler simulations, we are again testing to determine the Bayes factor of positive results, i.e. the factor by which we can increase our prior confidence that a positive connection effect exists in the direction of interest. We furthermore perform a sensitivity analysis with regards to significance level parameter α of the permutation test to create ROC curves to observe the trade-offs of increased sensitivity for decreased specificity with the proposed method.

3.7. Validation of PPI VGP-CCM Using a Face Perception Dataset

We perform PPI VGP-CCM to assess the connectivity between atlas parcellations defined by Destrieux and colleagues [8] in a face perception dataset [34], publicly available from http://data.pymvpa.org/datasets/haxby2001. MRI volumetric data is preprocessed using NiLearn's clean_img function, which comprises detrending, low-pass filtering and normalization to MNI space. The repetition time of the images was 2.5 seconds.

We perform analysis on data from parcellations of the cortical surface rather than volumetric regions of interest in order to finely parse cortical responses with minimal interference from white matter BOLD signal. The dataset, normalized to MNI space using NiLearn, is mapped to Freesurfer's "fsaverage" cortical surface (to which the Destrieux atlas is mapped) using the "vol_to_surf" command in NiLearn. Then, the BOLD signal in the surface vertices is deconvolved using a Fourier set and the hemodynamic response function described by Glover et al. [32].

The Fourier coefficients are determined in a regularized maximum a posteriori (MAP) approach defined in [31]. Concretely, we're determining the coefficients for a linear time invariant system:

$$Y = H\beta X + \epsilon \tag{12}$$

where H is the hemodynamic response convolution matrix in Toeplitz form, β are the Fourier coefficients, X is the matrix of Fourier bases, and ϵ is the error between the observed BOLD signal Y and the deconvolution model. The MAP solution to this system is:

$$\beta_{MAP} = (X^T H^T \Sigma^{-1} H X + \sigma^2 C_\beta^{-1})^{-1} X^T H^T \Sigma^{-1} Y \tag{13}$$

where C_β is a prior precision matrix, controlling the frequencies to attenuate in the deconvolution solution, Σ is the error correlation matrix, and σ is the error variance. Ordering the rows of the bases by ascending frequency (f), we define the a priori precision matrix with diagonal components equal to $1/f$ in order to prefer solutions concentrated with lower frequencies.

From the deconvolved BOLD signal, we make 2 psychophysiological interaction variables, similar to the approach used in the gPPI toolbox [44], based on the timestamps of the face and house events. We then perform the connectivity analysis for these two event types in the occipito-temporal cortical areas defined in Destrieux et al's atlas. Last, we contrast the connectivity values, $log(\kappa)$, and test whether connectivity is higher during presentation of face stimuli than during presentation of house objects. This is implemented using a one-sided Wilcoxon signed rank test on the group level (N=6), calculated for each element of the 46x46 connectivity matrices corresponding to the left and right occipito-temporal cortical parcels of the Destrieux atlas, i.e. the 46 parcels in the atlas whose label begin in "occipital", "oc-temp" and "temporal". The results of these tests were considered significant if the obtained p value was < 0.05 after correcting for 2116 multiple tests, using the proposed NBS approach (see above).

First, we expect, based on the literature on the neural mechanisms involved in face perception, that an area of the fusiform gyrus would contain distinct patterns of activity when faces were presented when compared to patterns of activity when houses were presented [34, 33]. We demonstrate this through searchlight information decoding in the occipito-temporal cortex, using searchlights with radii of 6mm [39] and a ridge classifier with a regularizer parameter $\alpha = 10$, as implemented in NiLearn. Accuracy maps are constructed per subject using

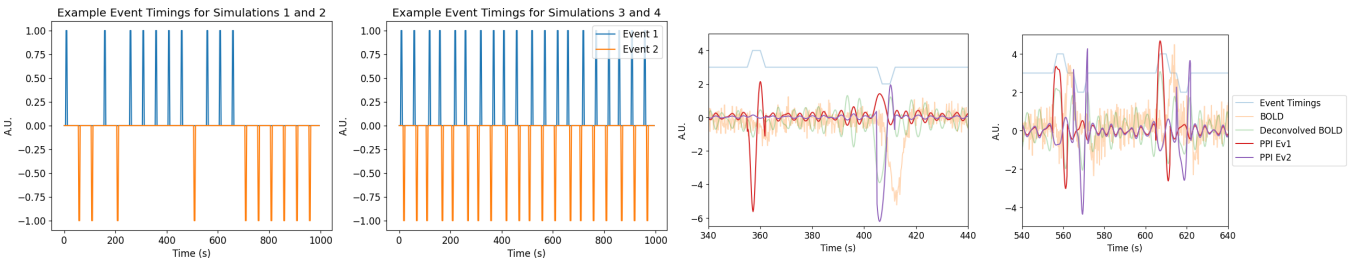

(a) (b) (c) (d)

Figure 3: Event timings for simulations 1 and 2 (a) and simulations 3 and 4 (b). Example processing to obtain PPI signals from deconvolved BOLD voxel signals for experiment 1 or 2 (c) and experiment 3 or 4 (d)

a leave-one-run-out cross-validation (there are 24 runs in the dataset). The threshold p for significance was $p_{FWE} < 0.05$, with cluster-wise correction for multiple comparisons across vertices using a Gaussian random field with a full-width-half-max of 20mm, based on a vertex-wise threshold of $p_{vertex} < 0.005$. We chose the relatively large value of 20mm in order to obtain conservative results.

Then, we expect our proposed method to reveal a directed connectivity from the occipital area to the fusiform and superior temporal areas, but we don't expect connectivity from the fusiform area to the superior temporal areas [12].

We exploit the proposed method by performing a PCA reduction of the vertex information of each parcel described in section 2.2 and subsequent state-space embedding reconstruction to perform pairwise connectivity analysis between parcels within the occipito-temporal cortex. As there are 46 parcels in the occipito-temporal cortex in the Destrieux atlas, we obtain a 46x46 connectivity matrix. NBS (described above) is exploited to identify face-sensitive parcels. To assess whether the connections are significantly stronger when viewing faces compared to houses in the surviving connections for face perception, a Wilcoxon signed rank test is performed. To compare the results of our method to an established procedure, we furthermore provide an analysis with PPI in its GLM form as outlined in [17] and [31]. Do note, PPI in its original form (unlike our proposed method) makes no inference on directional flow, rather it is a regression model that demonstrates whether a so-called "seed" explains the variance of other regions or voxels of interest differently depending on the state of a psychological variable of interest [47].

To validate the "network based statistic", we compare using two different null distributions that study the same effect (i.e. the nonparametric Wilcoxon signed rank test, and the binomial test with $H_o : \pi_o = 50\%$ and $H_1 : \pi_1 > 50\%$). Given adequate correction for multiple comparisons, these methods should yield the same connectivity results.

To demonstrate why they should give the same result, we look at what the Wilcoxon signed rank test performs. We have a random variable X we sample from, and we want to see if the median of this sample of random variable X is greater than 0. Lets, for example, say we have K observations X' of this random variable X (K subjects). To apply the Wilcoxon test, we first assign ranks R based on the **absolute value** of the samples X', in ascending order. For example, we have samples $X' = (-4, 11, -2, 1, 3, 10)$. The ranks would be $R = (4, 6, 2, 1, 3, 5)$. If there is ever a tie, let's say two observations X'_j and X'_i tie for the rank 3, the ranking takes the average, such that R_i and R_j would equal $\frac{3+4}{2}$. The Wilcoxon test then computes:

$$W = \sum_{k=0}^{K} sgn(X'_k) R_k \tag{14}$$

Where "sgn" is the sign function. A normal approximation can be used for the "null" distribution of the test statistic $\tilde{W}$, whose expectation is $E(\tilde{W}) = 0$ and variance is $Var(\tilde{W}) = \frac{K(K+1)(2K+1)}{6}$. We perform a 1 sided test to test whether our test statistic W is significantly greater than zero according to the null distribution $\tilde{W}$.

Consider positive results of coupling are 1 and negative values -1 (true or false); ranks are assigned based on their absolute value, and since they are all tied, the rank would all be 1. This, effectively, turns the statistic in to $W = \sum_{k^+}^{K^+} R^+ - \sum_{k^-}^{K^-} R^-$ (where R'^+ and K^+ are the positive ranks and number of positives respectively, and R^- and K^- are the negative ranks and number of negatives respectively). To test if this W is greater than zero can be seen as the same as asking whether the proportion of positive results is greater than 0.5, i.e. a coin flip, as $\frac{\sum_{k^+}^{K^+} R^+}{K} > 0.5$ if there are more positives than negatives. This is effectively equivalent to a test for a Binomial distribution that tests whether the probability of a "positive" test is greater than a coin flip, i.e. $H_o : \pi_o = 50\%$ and $H_1 : \pi_1 > 50\%$.

In order to benchmark the performance, we compare it to another family-wise multiple comparison correction method, false discovery rate (FDR). This method controls for the probability that q% of the statistical tests present type I errors, where q=5% for example. The explicit formula for false discovery rate, using the Benjamini-Horschberg procedure [5], is:

$$P(k) \leq \frac{k}{m} q \tag{15}$$

Where p values P are sorted in ascending order, k is the index of a specified p-value, and m is the number of tests performed. The procedure allows us to reject all the null hypothesis tested p(i) for i=1,2,...k that are greater that 0.05. Considering that the false discovery rate correction does not take into

consideration the structure of the network, while NBS does, we would expect that the Wilcoxon and Binomial tests will produce markedly different results.

4. Results

4.1. Rossler-Lorenz Systems

Coupling	$\epsilon_y = 1$	$\epsilon_y = 2$	$\epsilon_y = 3$	$\epsilon_y = 4$
Sensitivity	38%	32%	30%	42%
Bayes Factor|Specificity=98%	19	16	15	21

Table 2: Table of Bayes Factor for each coupling value ϵ_y. The specificity, found at $\epsilon_y = 0$, is 98%

In table 2 we see the Bayes factors and sensitivity for each coupling value. The specificity was calculated from zero coupling, which we arrived at 98% with only 1 false positive in 50 realizations. Though the sensitivity may appear low, the Bayes factor, as according to [36], shows that positive value from our model has strong strength of evidence ($BF > 10$) for all coupling values.

4.2. Network Coupling Deduced from Hemodynamics

	Condition 1			Condition 2			
	$N_1 \to N_2$	$N_2 \to N_1$	BF_{12}	$N_1 \to N_2$	$N_2 \to N_1$	BF_{21}	BF_{any}
Sim 1	77	1	77.0	35	17	0.48	4.35
Sim 2	76	4	19.0	1	78	78.0	30.8
Sim 3	74	4	18.5	39	19	0.48	3.58
Sim 4	75	1	75.0	3	78	26.0	38.3

Table 3: Results for directionality of the neurovascular system simulations. Simulation 1 and simulation 3 contain no induced directionality between any networks during condition 2; simulations 2 and 4 contain induced directionality from network 2 to network 1 during condition 2. All simulations contained induced coupling from network 1 to network 2 during condition 1. BF_{any} is calculated from the ratio of correct inferred direction to incorrectly inferred direction.

In table 3 we see the Bayes factors and number of accepted alternative hypothesis for each experiment. Considering there were 100 realizations for each simulation, the sensitivity appears generally over 70%. The worst specificity achieved for any of the simulations was 79%. The Bayes factor, as according to [36], shows that positive value from our model has strong strength of evidence ($BF > 10$) for experiments when both events induce coupling in one direction or the other, as seen in simulations 2 and 4. When one event induces no directional influence between either networks, as seen in simulations 1 and 3, the Bayes factor is reduced, however it still provides substantial evidence as according to [36].

In fig. 4 we demonstrate the sensitivity curve as a function of the first level significance level parameter α. In all simulations, we demonstrate an area under the curve (AUC) of over 0.7 for sensitivity of true coupling direction, while the false coupling detection all have an AUC of less than 0.5.

Parcel	Max T Score
Left G_occipital_sup	7.909
Left G_oc-temp_med-Lingual	5.853
Left G_oc-temp_med-Parahip	7.904
Left S_oc_middle_and_Lunatus	11.900
Left S_occipital_ant	4.217
Left S_temporal_inf	6.490
Left S_temporal_transverse	19.616
Right G_and_S_occipital_inf	6.142
Right G_oc-temp_lat-fusifor	6.372
Right G_oc-temp_med-Parahip	12.495
Right S_oc_middle_and_Lunatus	5.568
Right S_occipital_ant	4.158
Right S_temporal_inf	6.902
Right S_temporal_transverse	9.903

Table 4: Table of results from the searchlight decoding analysis after multiple comparisons correction with Gaussian random fields indicating the max group-level T-value statistic (decoding faces from houses above chance) obtained in each parcel of the Destrieux et al. atlas.

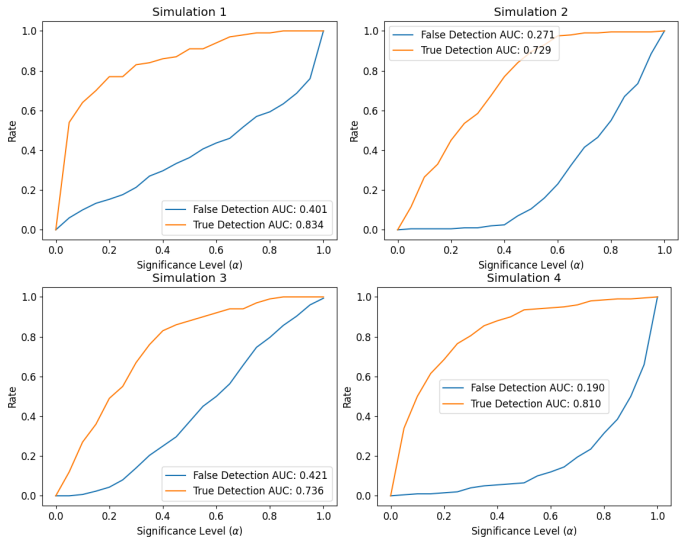

Figure 4: Sensitivity curves as a function of the first level significance level α for simulations 1 (a), 2 (b), 3 (c) and 4 (d).

4.3. Face Perception Dataset

In fig. 5 and table 4, we present group-level results from a searchlight decoding analysis in the occipito-temporal cortical regions. We note that, as expected based on previous findings, the inferior occipital cortex and the fusiform gyrus, particularly in the right hemisphere, contained activation patterns allowing to distinguish presentations of faces and houses above chance.

Fig. 6 shows a comparison of connectivity results obtained using either adjacency matrices created through a Wilcoxon signed rank test statistic, or the binomial statistic after NBS multiple comparison corrections. It can be seen that the results of the Wilcoxon null distribution and binomial null distribution contain much overlap, with only one connection uniquely detected using the binomial null distribution. These differences could be attributed to the slight differences in the null-distribution: Wilcoxon signed rank statistic uses a normal ap-

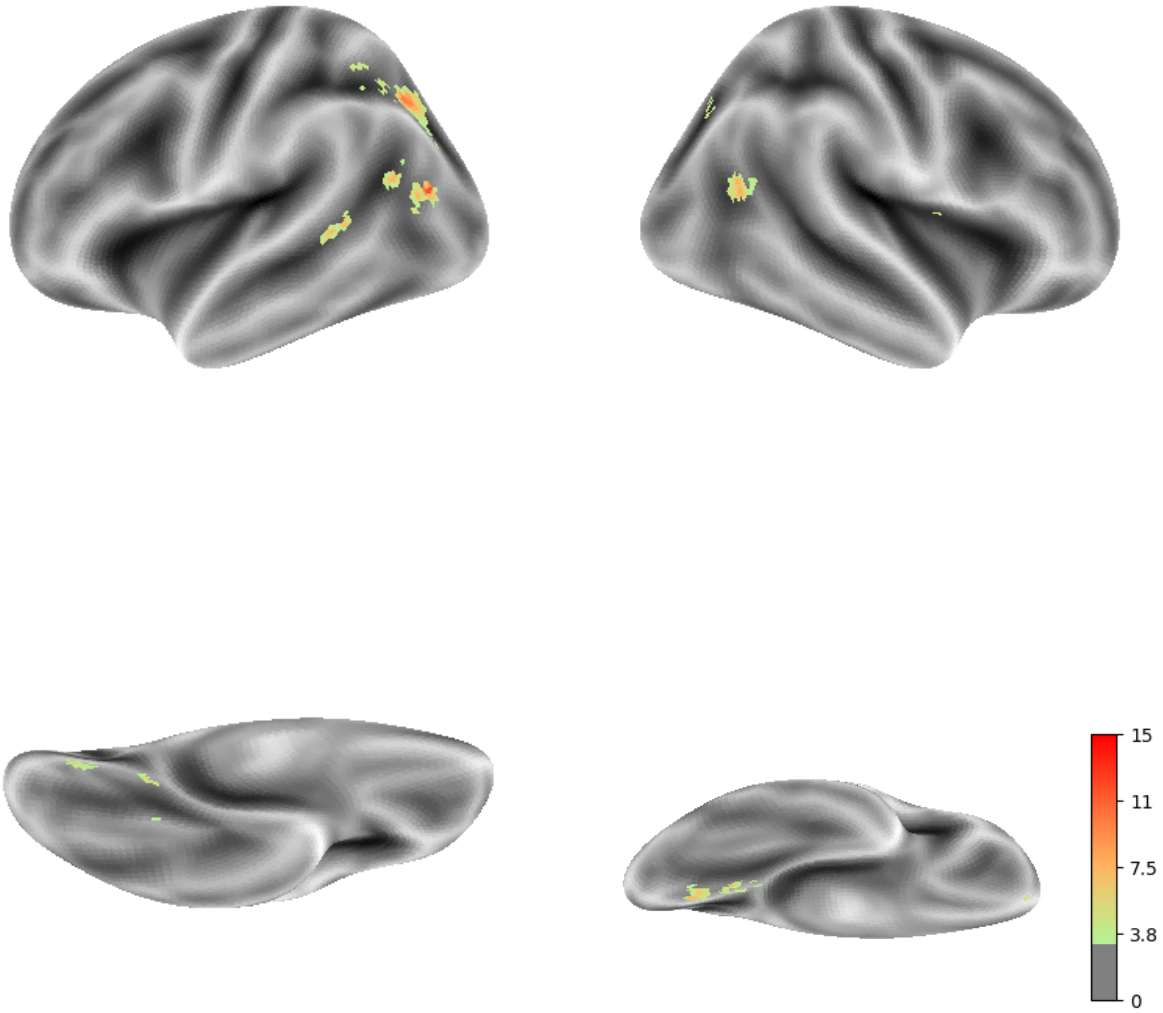

Figure 5: Results of searchlight decoding for discriminating when houses or faces were presented. Colored vertices represent the centers of searchlights in which the activation pattern allows to discriminate faces from houses above chance, based on a T-test across participants (N=6), thresholded at $p_{FWE} < 0.05$, with cluster-wise correction for multiple comparisons using Gaussian random fields. The top row presents lateral views of the cortex while the bottom row presents ventral views. The colorbar represents the T-statistic.

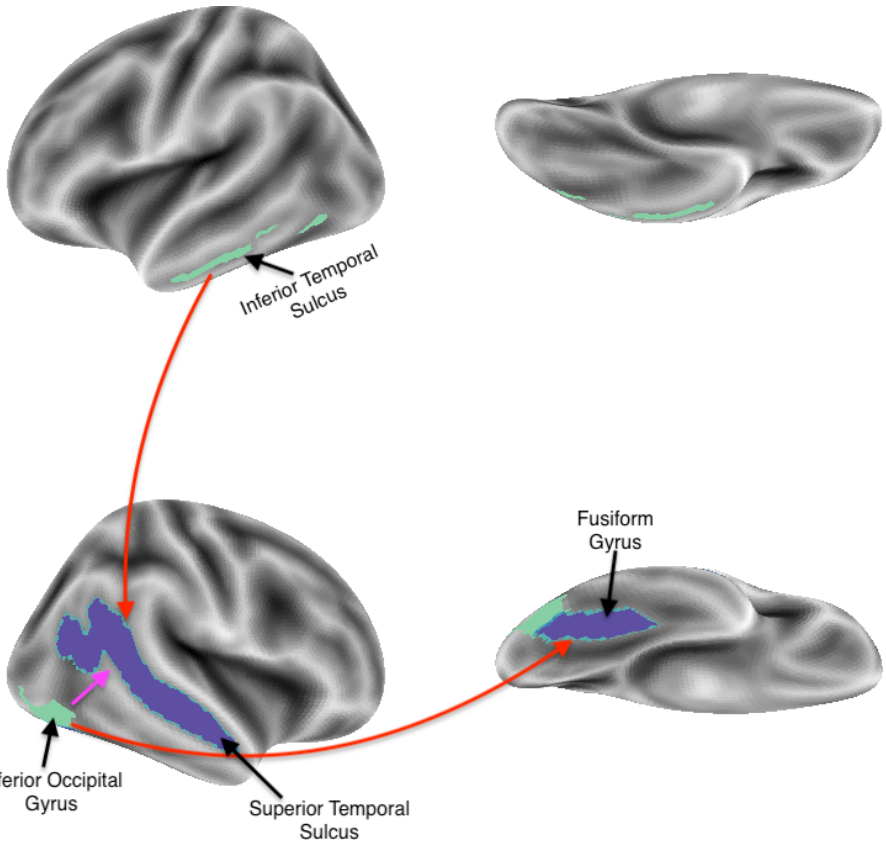

(a) PPI VGP-CCM

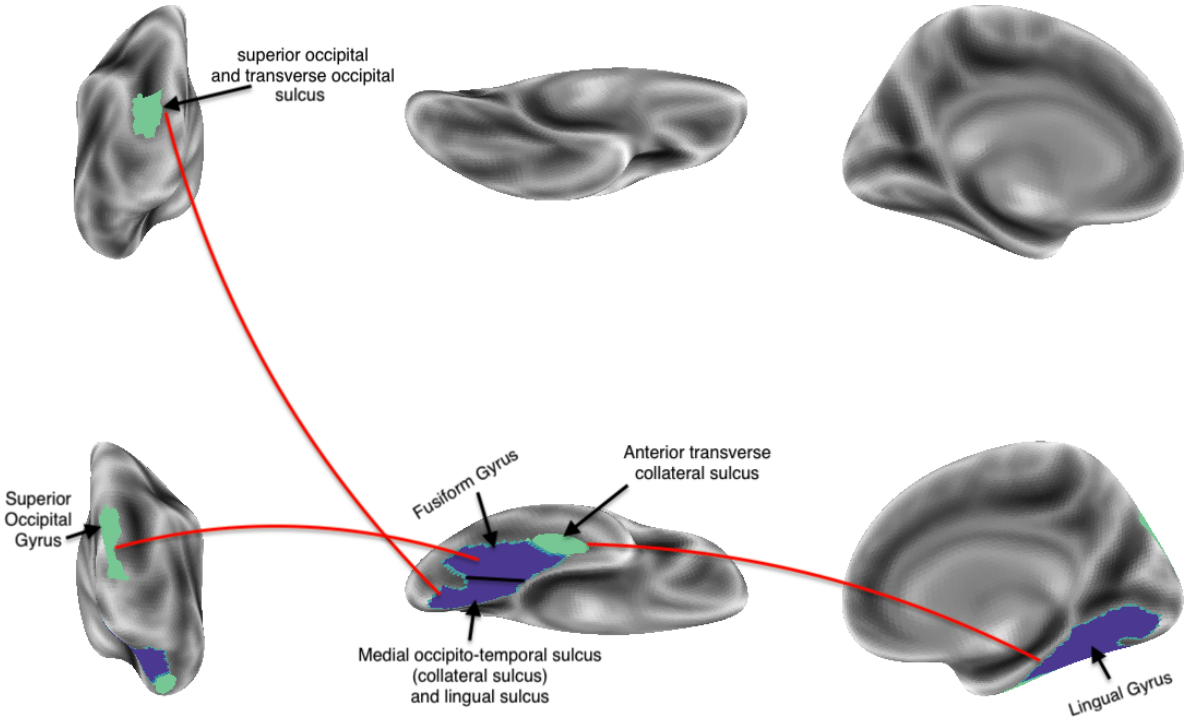

(b) Linear PPI

Figure 6: Results of the analysis of occipitotemporal cortex connectivity. Arrows indicate connections that are significantly stronger during presentation of face stimuli compared to house stimuli, assessed using the PPI-CCM method (a) or linear PPI (b). Results are shown after multiple comparisons correction using network based statistics (NBS). Arrows in red were discovered using either Wilcoxon or Binomial tests (results survive multiple comparisons; see methods), while the pink arrow was a connection uniquely identified using the Binomial test.

proximation, i.e. a continuous distribution, whereas the binomial is an exact discrete distribution.

Regarding the connectivity itself, fig. 6a demonstrates unique connectivity from the inferior occipital gyrus to the fusiform gyrus and to the superior temporal sulcus, without lateral connectivity between the fusiform gyrus and the superior temporal sulcus, agreeing with the DCM results in [12]. However, using PPI in its linear GLM form, seen in fig. 6b, we see superior occipital gyrus activity connecting with the fusiform gyrus. Furthermore, there are more connections uncovered by the linear PPI analysis that are not expected as according to the state-of-the-art results.

Fig. 7 demonstrates that with false discovery rate, we would find no significant connections using the Wilcoxon test instead of the binomial test, which would only allow significant discovery at p-value=0, which the binomial test permits given its discrete nature. On the other hand, using NBS multiple comparisons correction, with its consideration for network structure, permits a maximum p-value of 0.022 to pass.

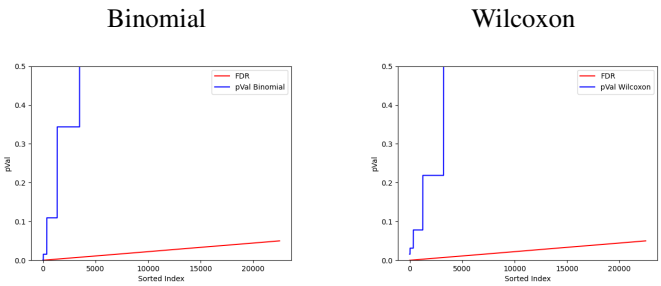

Figure 7: Displaying a sorted plot of p values in ascending order in blue, and the corresponding FDR control curve in red. The maximum value in which the p-values are below the FDR curve are chosen for the multiple comparison threshold. The panels demonstrate that results of the Wilcoxon test would never survive, whereas Binomial test results would only survive in the most extreme case of p-value = 0.

4.4. Discussion

In this paper, we describe and test a novel method for uncovering connectivity during tasks while taking into consideration contextual dependence in state space by extending the Gaussian Processes Convergent Cross-Mapping with a non-stationary covariance functions for psychophysiological interactions dictated by the physiological signal. We verified the strength of evidence for a positive result using simulations of bidirectional Rossler-Lorenz and neurovascular systems of equations. We furthermore test whether the proposed method can uncover previously documented effective connectivity during a face perception task.

Simulations revealed Bayes factors that exceed substantial strength of evidence. This result indicates that in the event that a positive connectivity is reported, our knowledge about the connectivity increases substantially [36].

While sensitivity analyses yielded a low value, negative results do not substantially decrease our odds of identifying a connection. For example, if we calculated the Bayes factor for negative results, i.e. $BF(-) = \frac{p(-|M=-)}{p(+|M=-)}$ for $\epsilon_y = 4 : 42\%$, would be 1.69. This value means that obtaining a negative result could, at the most, less than double our confidence about the absence of a connection.

Let's assume we collected 20 pairs of time-series with unknown coupling, as if we sampled 20 subjects from a population, and we place odds of there being a connection between the time-series at 1:999, i.e. a prevalence of 0.1%. Let's also assume that our analysis yields 5 positive and 15 negative outcomes, an unlikely outcome given the low prevalence. In this case, the a posteriori odds would be $1 \cdot 21^5 : 999 \cdot 1.69^{15}$ or 61% probability of there actually being a connection. Thus, false positive results from this method do not yield clear evidence about unlikely connections.

We note that these are simulations where the system's equations we are comparing can be parcellated exactly, i.e. we determine the Rossler time series and the Lorenz series to create the shadow manifold in cross-mapping. However, biological systems and fMRI BOLD data contain substantial variance, due to mislocalization of neural activity estimated from BOLD signals (BOLD signals are dominated by large blood vessels, which are not located within the active neural tissue) [35]. To avoid deriving overly strong inferences from false positive results, we propose to perform a binomial test, with a null hypothesis of $\pi_o = 50\%$ and alternate hypothesis $\pi_o > 50\%$.

Regarding the results for the network coupling deduced from hemodynamics in tab 3, we noticed that in all cases PPI VGP-CCM provides substantial strength of evidence for deducing true coupling directions. However, curiously, for simulations with a condition when no coupling was invoked (simulation 1 and 3, condition 2), the Bayes factor decreased. This may be explained by fig. 2; i.e., the sensitivity to difference of entropy during the condition 1 may have been reduced significantly when exploring condition 2, however no substantial amount of difference of entropy was observed in condition 2. This may lead the PPI VGP-CCM, if sensitive enough, to detect significant changes in a posteriori entropy leaking from condition 1 to condition 2. Nevertheless, considering on a group level we try to reject the binomial null hypothesis $H_o : \pi_o = 50\%$ and accept $H_1 : \pi_1 > 50\%$, condition 2 never presents greater than a 50% rate of positive results during simulations 1 and 3, thus will not present significant effects on a group level. Fig. 4 further demonstrates the power of PPI VGP-CCM of detecting true coupling with high sensitivity while maintaining specificity. The result shows that a first level analysis may permit higher α, substantially increasing sensitivity while keeping subject level specificity $(1 - FPR)$ greater than 50% in order that the second level tests for coupling may maintain specificity.

In order to assess the performance of our method on empirical data, we aimed to replicate previously documented directed functional connectivity findings about face perception using a validated dataset. We first replicated the classic finding that presentations of face and house stimuli can be decoded from BOLD signal data, particularly in the right hemisphere [34, 33], by training a classifier on the BOLD signal patterns obtained in occipital gyrus and fusiform gyrus. Our connectivity analysis, constrained to occipital and temporal cortical regions, revealed that the superior temporal sulcus and the fusiform gyrus

uniquely received information from inferior occipital cortical areas, and we found no connectivity between superior temporal sulcus and the fusiform gyrus, as seen in fig. 6a. By contrast, the results of a PPI analysis in its original linear GLM form 6b, run on the same data, revealed a connection between the superior, but not the inferior, occipital area to the fusiform gyrus, a result incongruent with previous findings. This analysis further revealed connectivity with other occipito-temporal cortical areas not traditionally associated with face perception. This result further illustrates PPI VGP-CCM's performance for detecting connectivity in fMRI datasets.

We note that we used a deconvolution procedure to evaluate functional connectivity based on the fMRI data, to align the timing of the psychological events with the neural data inferred from the observed BOLD signal [31]. An alternate approach to creating a psychophysiological variable may have been to multiply the non-deconvolved BOLD signal with the variable of event timings convolved with the hemodynamic response [17], an approach we define as the "convolutional model of PPI VGP-CCM". We demonstrate the effect of so-called convolutional models in Appendix A fig. A.8. The results of convolutional models of PPI VGP-CCM analysis reveal a connection between the middle occipital gyrus, the fusiform and superior temporal gyri. While there are reports of involvement of the middle occipital gyrus in face perception [26, 46, 45], this involvement appears more restricted to high level processing. For example, the middle occipital gyrus has been shown to be sensitive to dynamic effects in face perception [37]. The difference between the results obtained with convolutional models of PPI VGP-CCM analysis and the suggested deconvolutional approach in the main text illustrate the importance of deconvolution to obtain results with reliable temporal specificity.

Furthermore, we display that network based statistics are robust in terms of determining the proper threshold for controlling family-wise error rate, where it reveals common networks even when the null-distribution is improperly selected for the test at hand. To compare, we show naive approaches to multiple comparison correction such as false discovery rate (fig. 7) can be far too conservative in comparison to network-based statistics. Given that the Wilcoxon test uses a normal continuous distribution approximation for its null distribution, p-values will always be strictly greater than 0 . With the statistical expected value of the null distribution $E(W) = \frac{K(K+1)}{4}$ and variance $Var(W) = \frac{K(K+1)(2K+1)}{24}$, even if the analysis of the data of every single subject would give positive results, we would obtain a p-value of 0.0139, a value that would never be significant with FDR correction (fig. 7); this may instead be significant when considering this value comes from its own network that we are ultimately determining the significance of, i.e. looking at network scale statistical structures in a similar way that a Gaussian random field looks at spatial statistical structures of clusters for multiple comparison corrections. False discovery rate's structure agnostic nature does not permit it to have power to detect such effect.

Time-lag based methods of connectivity in fMRI analysis have been often discredited considering the sluggish nature of BOLD signals, as well as the nonlinear effects that time-constants may have on delayed neurovascular response [21, 22, 7]. For this reason, generative models in the vein of dynamic causal models have been preferred in neuroimaging literature [18, 52, 13]. GP-CCM and the proposed method in this paper, PPI VGP-CCM, attempt to mitigate limitations of time-lag based methods by imposing prior Gaussian process constraints to lift time-lag methods to a generative statistical model of the state space manifold for nonparametric model evidence comparisons. As formulated here, this results in combinatorial pair-wise model evidence comparisons between regions of interests, i.e. parcellations of the cortex in our case. However, it is understood that the brain contains a slew of recurrent networks [56, 6, 27], paths of information that result in indirect coupling [48], and phenomena emerging from high-order statistical behaviors such as redundancy and synergy [4, 41]. Thus, to further understand complex networks associated with phenomena such as consciousness, such properties may need to be integrated into the proposed method. This is partly a challenge considering the proposed method is primarily functional, rather than effective; in other words it is concerned with statistical properties of relationships between time series, but disregards structural properties such as white matter tracts [19]. Future work to overcome these limitations may be directed towards integrating a set of conditional independence tests for regularizing network graphs uncovered by VGP-CCM to account for indirect connectivity [49], constructing hypergraphs by determining interactions between clusters of brain regions/parcels for parsing high order behavior [4, 41] or instituting structural priors in the method to lift it to effective measures.

To conclude, we demonstrate a novel method to augment the covariance function in VGP-CCM to permit task-dependent connectivity analysis, exploiting psychophysiological interaction theory. We show that the method provides substantial strength of evidence about directional connectivity between pairs of regions, through simulations of coupled chaotic systems and through neural networks observed by hemodynamics. Furthermore, the proposed method uncovers previously described connections associated with face perception in the ventrolateral occipito-temporal cortex. Our method may thus be useful for performing pairwise directional influence tests in order to uncover interactions between regions of interest in the brain.

5. Acknowledgement

This study was financed in part by the European Commission Horizon 2020 project RHUMBO, grant agreement ID 813234, DOI: 10.3030/813234., and by the Italian Ministry of Education and Research (MIUR) in the framework of the Cross-Lab project (Departments of Excellence).

References

[1] Aggarwal, C. C., Hinneburg, A., and Keim, D. A. (2001). On the surprising behavior of distance metrics in high dimensional space. In Van den Bussche, J. and Vianu, V., editors, *Database Theory — ICDT 2001*, pages 420–434, Berlin, Heidelberg. Springer Berlin Heidelberg.

[2] Ahmed, N. A. and Gokhale, D. (1989). Entropy expressions and their estimators for multivariate distributions. *IEEE Transactions on Information Theory*, 35(3):688–692.

[3] Bartolovic, N., Gross, M., and Günther, T. (2020). Phase space projection of dynamical systems. *Computer Graphics Forum*, 39(3):253–264.

[4] Battiston, F., Amico, E., Barrat, A., Bianconi, G., Ferraz de Arruda, G., Franceschiello, B., Iacopini, I., Kéfi, S., Latora, V., Moreno, Y., et al. (2021). The physics of higher-order interactions in complex systems. *Nature Physics*, 17(10):1093–1098.

[5] Benjamini, Y. and Hochberg, Y. (1995). Controlling the false discovery rate: a practical and powerful approach to multiple testing. *Journal of the Royal statistical society: series B (Methodological)*, 57(1):289–300.

[6] Dehaene, S. and Changeux, J.-P. (2011). Experimental and theoretical approaches to conscious processing. *Neuron*, 70(2):200–227.

[7] Deshpande, G., Sathian, K., and Hu, X. (2010). Effect of hemodynamic variability on granger causality analysis of fmri. *Neuroimage*, 52(3):884–896.

[8] Destrieux, C., Fischl, B., Dale, A., and Halgren, E. (2010). Automatic parcellation of human cortical gyri and sulci using standard anatomical nomenclature. *NeuroImage*, 53(1):1–15. 20547229[pmid].

[9] Deyle, E. R. and Sugihara, G. (2011). Generalized theorems for nonlinear state space reconstruction. *PLOS ONE*, 6(3):1–8.

[10] Ding, M., Bressler, S. L., Yang, W., and Liang, H. (2000). Short-window spectral analysis of cortical event-related potentials by adaptive multivariate autoregressive modeling: data preprocessing, model validation, and variability assessment. *Biol Cybern*, 83(1):35–45.

[11] Efron, B. and Tibshirani, R. J. (1994). *An introduction to the bootstrap*. CRC press.

[12] Fairhall, S. L. and Ishai, A. (2007). Effective connectivity within the distributed cortical network for face perception. *Cerebral cortex*, 17(10):2400–2406.

[13] Frässle, S., Harrison, S. J., Heinzle, J., Clementz, B. A., Tamminga, C. A., Sweeney, J. A., Gershon, E. S., Keshavan, M. S., Pearlson, G. D., Powers, A., et al. (2021). Regression dynamic causal modeling for resting-state fmri. *Human brain mapping*, 42(7):2159–2180.

[14] Frässle, S., Lomakina, E. I., Razi, A., Friston, K. J., Buhmann, J. M., and Stephan, K. E. (2017). Regression dcm for fmri. *Neuroimage*, 155:406–421.

[15] Friston, K. (2009). Causal modelling and brain connectivity in functional magnetic resonance imaging. *PLoS biology*, 7(2):e1000033.

[16] Friston, K. (2011a). Dynamic causal modeling and granger causality comments on: the identification of interacting networks in the brain using fmri: model selection, causality and deconvolution. *NeuroImage*, 58(2):303–311.

[17] Friston, K., Buechel, C., Fink, G., Morris, J., Rolls, E., and Dolan, R. (1997). Psychophysiological and modulatory interactions in neuroimaging. *NeuroImage*, 6(3):218–229.

[18] Friston, K., Harrison, L., and Penny, W. (2003). Dynamic causal modelling. *NeuroImage*, 19(4):1273 – 1302.

[19] Friston, K., Moran, R., and Seth, A. K. (2013). Analysing connectivity with granger causality and dynamic causal modelling. *Current opinion in neurobiology*, 23(2):172–178.

[20] Friston, K. J. (1994). Functional and effective connectivity in neuroimaging: a synthesis. *Human brain mapping*, 2(1-2):56–78.

[21] Friston, K. J. (2011b). Functional and effective connectivity: a review. *Brain connectivity*, 1(1):13–36.

[22] Friston, K. J., Bastos, A. M., Oswal, A., van Wijk, B., Richter, C., and Litvak, V. (2014). Granger causality revisited. *NeuroImage*, 101:796–808. 25003817[pmid].

[23] Friston, K. J., Fletcher, P., Josephs, O., Holmes, A., Rugg, M., and Turner, R. (1998). Event-related fmri: characterizing differential responses. *Neuroimage*, 7(1):30–40.

[24] Friston, K. J., Jezzard, P., and Turner, R. (1994). Analysis of functional mri time-series. *Human brain mapping*, 1(2):153–171.

[25] Friston, K. J. and Price, C. J. (2003). Degeneracy and redundancy in cognitive anatomy. *Trends in Cognitive Sciences*, 7(4):151–152.

[26] Fusar-Poli, P., Placentino, A., Carletti, F., Allen, P., Landi, P., Abbamonte, M., Barale, F., Perez, J., McGuire, P., and Politi, P. (2009). Laterality effect on emotional faces processing: Ale meta-analysis of evidence. *Neuroscience letters*, 452(3):262–267.

[27] Garrido, M. I., Kilner, J. M., Kiebel, S. J., and Friston, K. J. (2007). Evoked brain responses are generated by feedback loops. *Proceedings of the National Academy of Sciences*, 104(52):20961–20966.

[28] Gatica, M., Cofré, R., Mediano, P. A., Rosas, F. E., Orio, P., Diez, I., Swinnen, S. P., and Cortes, J. M. (2021). High-order interdependencies in the aging brain. *Brain Connectivity*, 11(9):734–744.

[29] Ghouse, A., Faes, L., and Valenza, G. (2021). Inferring directionality of coupled dynamical systems using gaussian process priors: Application on neurovascular systems. *Phys. Rev. E*, 104:064208.

[30] Ghouse, A. and Valenza, G. (2022). Inferring parsimonious coupling statistics in nonlinear dynamics with variational gaussian processes. In *2022 30th European Signal Processing Conference (EUSIPCO)*.

[31] Gitelman, D. R., Penny, W. D., Ashburner, J., and Friston, K. J. (2003). Modeling regional and psychophysiologic interactions in fmri: the importance of hemodynamic deconvolution. *Neuroimage*, 19(1):200–207.

[32] Glover, G. H. (1999). Deconvolution of impulse response in event-related bold fmri1. *NeuroImage*, 9(4):416–429.

[33] Hanson, S. J., Matsuka, T., and Haxby, J. V. (2004). Combinatorial codes in ventral temporal lobe for object recognition: Haxby (2001) revisited: is there a "face" area? *Neuroimage*, 23(1):156–166.

[34] Haxby, J. V., Gobbini, M. I., Furey, M. L., Ishai, A., Schouten, J. L., and Pietrini, P. (2001). Distributed and overlapping representations of faces and objects in ventral temporal cortex. *Science*, 293(5539):2425–2430.

[35] Hillman, E. M. (2014). Coupling mechanism and significance of the bold signal: a status report. *Annual review of neuroscience*, 37:161.

[36] Jeffreys, H. (1998). *The theory of probability*. OUP Oxford.

[37] Joseph, J. E., Gathers, A. D., Liu, X., Corbly, C. R., Whitaker, S. K., and Bhatt, R. S. (2006). Neural developmental changes in processing inverted faces. *Cognitive, Affective, & Behavioral Neuroscience*, 6(3):223–235.

[38] Kim, J., Wozniak, J. R., Mueller, B. A., Shen, X., and Pan, W. (2014). Comparison of statistical tests for group differences in brain functional networks. *NeuroImage*, 101:681–694.

[39] Kriegeskorte, N., Goebel, R., and Bandettini, P. (2006). Information-based functional brain mapping. *Proceedings of the National Academy of Sciences*, 103(10):3863–3868.

[40] Latham, P. E. and Nirenberg, S. (2005). Synergy, redundancy, and independence in population codes, revisited. *Journal of Neuroscience*, 25(21):5195–5206.

[41] Luppi, A. I., Mediano, P. A., Rosas, F. E., Holland, N., Fryer, T. D., O'Brien, J. T., Rowe, J. B., Menon, D. K., Bor, D., and Stamatakis, E. A. (2022). A synergistic core for human brain evolution and cognition. *Nature Neuroscience*, 25(6):771–782.

[42] MacKay, D. J. C. (1996). *Bayesian Methods for Backpropagation Networks*, pages 211–254. Springer New York, New York, NY.

[43] McInnes, L., Healy, J., and Melville, J. (2018). Umap: Uniform manifold approximation and projection for dimension reduction. *arXiv preprint arXiv:1802.03426*.

[44] McLaren, D. G., Ries, M. L., Xu, G., and Johnson, S. C. (2012). A generalized form of context-dependent psychophysiological interactions (gppi): a comparison to standard approaches. *Neuroimage*, 61(4):1277–1286.

[45] Minnebusch, D. A., Suchan, B., Köster, O., and Daum, I. (2009). A bilateral occipitotemporal network mediates face perception. *Behavioural brain research*, 198(1):179–185.

[46] Nagy, K., Greenlee, M. W., and Kovács, G. (2012). The lateral occipital cortex in the face perception network: an effective connectivity study. *Frontiers in psychology*, 3:141.

[47] O'Reilly, J. X., Woolrich, M. W., Behrens, T. E., Smith, S. M., and Johansen-Berg, H. (2012). Tools of the trade: psychophysiological interactions and functional connectivity. *Social cognitive and affective neuroscience*, 7(5):604–609.

[48] Ross, L. N. (2020). Causal concepts in biology: How pathways differ from mechanisms and why it matters. *The British Journal for the Philosophy of Science*.

[49] Runge, J., Nowack, P., Kretschmer, M., Flaxman, S., and Sejdinovic, D. (2019). Detecting and quantifying causal associations in large nonlinear time series datasets. *Science advances*, 5(11):eaau4996.

[50] Smirnov, D. A. (2013). Spurious causalities with transfer entropy. *Phys. Rev. E*, 87:042917.

[51] Smirnov, D. A. and Bezruchko, B. P. (2012). Spurious causalities due to low temporal resolution: Towards detection of bidirectional coupling from time series. 100(1):10005.

[52] Stephan, K. E., Weiskopf, N., Drysdale, P. M., Robinson, P. A., and Friston, K. J. (2007). Comparing hemodynamic models with dcm. *Neuroimage*,

38(3):387–401.
[53] Stramaglia, S., Angelini, L., Wu, G., Cortes, J. M., Faes, L., and Marinazzo, D. (2016). Synergetic and redundant information flow detected by unnormalized granger causality: Application to resting state fmri. *IEEE Transactions on Biomedical Engineering*, 63(12):2518–2524.
[54] Sugihara, G., May, R., Ye, H., Hsieh, C.-h., Deyle, E., Fogarty, M., and Munch, S. (2012). Detecting causality in complex ecosystems. *Science*, 338(6106):496–500.
[55] Szubert, B., Cole, J. E., Monaco, C., and Drozdov, I. (2019). Structure-preserving visualisation of high dimensional single-cell datasets. *Scientific reports*, 9(1):1–10.
[56] Tononi, G. and Edelman, G. M. (1998). Consciousness and complexity. *science*, 282(5395):1846–1851.
[57] Wen, X., Yao, L., Liu, Y., and Ding, M. (2012). Causal interactions in attention networks predict behavioral performance. *Journal of Neuroscience*, 32(4):1284–1292.
[58] Zalesky, A., Fornito, A., and Bullmore, E. T. (2010). Network-based statistic: identifying differences in brain networks. *Neuroimage*, 53(4):1197–1207.
[59] Zeidman, P., Jafarian, A., Seghier, M. L., Litvak, V., Cagnan, H., Price, C. J., and Friston, K. J. (2019). A guide to group effective connectivity analysis, part 2: Second level analysis with peb. *NeuroImage*, 200:12–25.
[60] Zhou, Z., Wang, X., Klahr, N. J., Liu, W., Arias, D., Liu, H., von Deneen, K. M., Wen, Y., Lu, Z., Xu, D., et al. (2011). A conditional granger causality model approach for group analysis in functional magnetic resonance imaging. *Magnetic resonance imaging*, 29(3):418–433.

Appendix A. Consequences of Using Convolution models Instead of Deconvolution for Constructing Psychophysiological Interaction Variables

Below, we plot the effects of convolutional models of PP on the assessment of connectivity using PPI VGP-CCM. Notice that indeed, the occipital face area has centralized forward connectivity to the ventrolateral face perception network at the middle occipital gyrus rather than the inferior occipital gyrus, demonstrating that convolutional models of PP show effects that lag the true connectivity timings of interest, as uncovered by deconvolutional models seen in 6, i.e. the inferior occipital gyrus as the main source of information to the ventrolateral network.

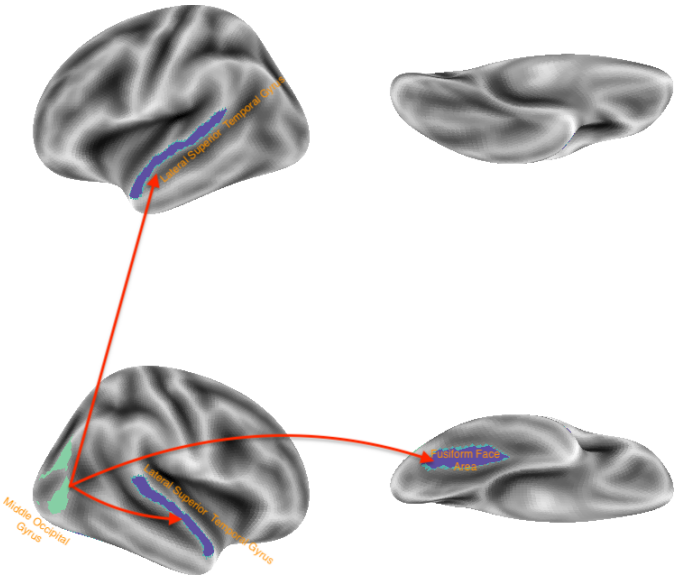

Figure A.8: Effect of using convolution models for PP variables on connectivity matrices, with multiple comparisons corrections using the binomial distribution for the group-level null-distribution. Make note that the middle occipital gyrus is instead the main source of information to the ventrolateral face perception network, rather than the inferior occipital gyrus that is to be expected.